

# RadioLLM: Introducing Large Language Model into Cognitive Radio via Hybrid Prompt and Token Reprogrammings

Shuai Chen<sup>1</sup>, Yong Zu<sup>1</sup>, Zhixi Feng<sup>1</sup>, Shuyuan Yang<sup>1</sup>, Mengchang Li<sup>1</sup>, Yue Ma<sup>1</sup>, Jun Liu<sup>1</sup>, Qiukai Pan<sup>1</sup>, Xinlei Zhang<sup>1</sup>, Changjun Sun<sup>1</sup>

<sup>1</sup>Xidian University

shuai\_chen@stu.xidian.edu.cn, yzuwork@stu.xidian.edu.cn, zxfeng@xidian.edu.cn, syyang@xidian.edu.cn, mengchangli@stu.xidian.edu.cn, mayue@xidian.edu.cn, jun\_liu@stu.xidian.edu.cn, panqiukai@stu.xidian.edu.cn, xlzhang1@stu.xidian.edu.cn, sunchangjun@stu.xidian.edu.cn

## Abstract

The increasing scarcity of spectrum resources and the rapid growth of wireless device have made efficient management of radio networks a critical challenge. Cognitive Radio Technology (CRT), when integrated with deep learning (DL), offers promising solutions for tasks such as radio signal classification (RSC), signal denoising, and spectrum allocation. However, existing DL-based CRT frameworks are often task-specific and lack scalability to diverse real-world scenarios. Meanwhile, Large Language Models (LLMs) have demonstrated exceptional generalization capabilities across multiple domains, making them a potential candidate for advancing CRT technologies. In this paper, we introduce RadioLLM, a novel framework that incorporates Hybrid Prompt and Token Reprogramming (HPTR) and a Frequency Attuned Fusion (FAF) module to enhance LLMs for CRT tasks. HPTR enables the integration of radio signal features with expert knowledge, while FAF improves the modeling of high-frequency features critical for precise signal processing. These innovations allow RadioLLM to handle diverse CRT tasks, bridging the gap between LLMs and traditional signal processing methods. Extensive empirical studies on multiple benchmark datasets demonstrate that the proposed RadioLLM achieves superior performance over current baselines.

## 1 Introduction

With the proliferation of wireless devices and the scarcity of spectrum resources, managing and optimizing limited wireless network resources has become increasingly challenging [Nahum *et al.*, 2023], [Sathyanarayanan *et al.*, 2023a]. Integrating artificial intelligence (AI) with cognitive radio technology (CRT) offers a promising solution for optimizing spectrum sharing and enhancing communication quality [Haider *et al.*, 2015]. However, traditional machine learning (ML) methods for radio cognition are limited by device noise and interference [Feng *et al.*, 2024], while deep learning (DL) approaches, driven by data, excel at tasks like radio signal

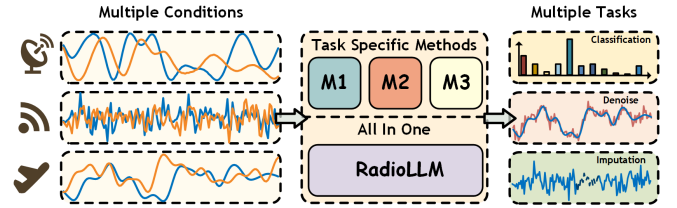


Figure 1: Comparison of existing CRT frameworks with our proposed approach.

classification (RSC), signal denoising, and spectrum allocation, significantly improving communication performance.

DL-based CRT frameworks simplify system complexity through end-to-end training but are often tailored to specific tasks and signal types. As shown in Figure 1, deploying these frameworks in real-world scenarios requires task-specific configurations, which limits their scalability and application in diverse industrial environments. Developing a universal CRT framework capable of handling diverse tasks and signals remains a critical challenge.

The advent of LLMs has reignited interest in Artificial General Intelligence (AGI). LLMs, pretrained on large-scale datasets using autoregressive techniques, demonstrate generalization capabilities far beyond traditional models, making them promising for CRT. Despite their potential, LLMs face challenges in CRT applications, such as the need for significant computational resources and architectures tailored to radio signals.

Although LLMs have been applied to semantic communication [Xie *et al.*, 2024], network optimization [Kotaru, 2023], and spectrum sensing [Shao *et al.*, 2024], current methods exhibit several limitations:

**1) Limited Cognitive Understanding of Radio Signals:** LLMs, trained on text, lack inherent understanding of radio signals. Existing works rely on text-based prompts and external tools, limiting their ability to process raw signals. We adopt reprogramming techniques in [Jin *et al.*, 2024] to transform radio signals into formats compatible with LLM input, enabling direct signal processing and improving cognitive capabilities.

**2) Inefficient Expert Knowledge Integration:** Textual prompting for injecting expert knowledge often results in ver-

bose templates with unnecessary words, increasing computational overhead [Jin *et al.*, 2024]. We propose a hybrid prompting method that retrieves concise and contextually relevant tokens, reducing memory usage and runtime while preserving information richness.

**3) Challenges in Capturing High-Frequency Signal Features:** LLMs excel at low-frequency global information but struggle with high-frequency details critical for precise RSC tasks [Bai *et al.*, 2022], [Si *et al.*, 2022]. To address this, we propose the Frequency Attuned Fusion (FAF) module, which combines high-frequency features from CNNs with the global context captured by LLMs, enhancing their performance in RSC tasks.

In this paper, we introduce RadioLLM, which integrates Hybrid Prompt and Token Reprogramming (HPTR) with CRT using LLMs. HPTR couples expert knowledge with radio signal features, leveraging LLMs’ world knowledge for semantic and high-dimensional feature extraction. Additionally, the FAF module improves the modeling of high-frequency information, while a lightweight decoder maps features back to the original signal space. Our contributions include:

1. We propose a novel multimodal RadioLLM that achieves versatile CRT applications across diverse scenarios through multi-task joint learning. Leveraging the LLM’s inherently rich world knowledge, we explore its application in CRT by employing reprogramming techniques. This approach enables the direct processing of radio signals by the LLM, significantly enhancing its cognitive capabilities regarding diverse signal types and reducing reliance on manual prompt engineering.
2. To mitigate computational overhead and memory consumption, we introduce an innovative hybrid prompt technique that combines software and hardware prompts. This method involves identifying the top K semantically similar anchors within a joint semantic space for template text prompt embeddings. These anchors serve as concise and contextually relevant prompts, effectively eliminating unnecessary filler words while maintaining strong correlations with signal features. This streamlined prompting technique optimizes the model’s performance in CRT tasks by ensuring that the prompts are both succinct and rich in pertinent information.
3. We designed the FAF module to enhance the LLM’s ability to model high-frequency features by fusing high-frequency and low-frequency information, thereby improving the performance of the downstream classification task while ensuring the performance of the generation task.

## 2 RELATED WORK

### 2.1 Traditional DL-Based CRT Framework

Deep learning (DL)-based methods have been widely applied to critical tasks in CRT, such as RSC, signal denoising, and signal recovery. In RSC, supervised learning (SL) approaches have shown significant progress. For example, PETCGDNN

used CNNs and GRUs for feature extraction to build an efficient modulation recognition model [Zhang *et al.*, 2021a]. Additionally, a multi-view fusion RSC method was proposed, which leverages features from the time, frequency, and time-frequency domains to enhance performance [Ke and Vikalo, 2021].

The challenge of obtaining high-quality labeled data in wireless communication has driven the adoption of self-supervised learning (SSL). A Transformer-based SSL framework, TCSSAMR, was proposed for RSC [Kong *et al.*, 2023a], and MCLHN utilized masked contrastive learning with hard negatives to enhance signal diversity [Xiao *et al.*, 2024]. For signal denoising and partial recovery, a Deep Denoising Network was proposed using residual learning [Kaushal *et al.*, 2016], and a time-frequency domain autoencoder was developed for denoising [Chen *et al.*, 2024].

While these methods excel in specific tasks, they are limited to individual applications and specific data types. To address this, we propose the LLM architecture as a universal CRT framework, pioneering AGI applications in CRT.

### 2.2 Previous LLM-Based CRT Framework

The emergence of LLMs has brought significant advancements to AI, influencing domains such as time series analysis and CRT. For example, LLMs have been used in semantic communication systems for contextual understanding [Xie *et al.*, 2024] and in 6G edge computing for user association and resource allocation [Kotaru, 2023]. However, these applications are mostly limited to telecommunications language understanding.

WirelessLLM has extended LLM applications to CRT tasks like power allocation and spectrum sensing, advancing AGI integration in CRT [Shao *et al.*, 2024]. Yet, it relies on external tools, lacks an end-to-end signal processing pipeline, and overlooks critical tasks like WSC and signal denoising.

To overcome these challenges, we build on recent advances in time-series LLM research [Jin *et al.*, 2024], [Pan *et al.*, 2024], [Cao *et al.*, 2024] by incorporating reprogramming and hybrid prompting techniques. This enables the development of a unified and versatile CRT framework capable of handling diverse signal types and tasks.

## 3 Methodology

**Overview:** As shown in Figure 2, RadioLLM is designed with two primary components. First, the input radio signal is divided into patches to generate its signal embedding. The first component involves combining expert knowledge prompts with the top-K semantically similar anchors, retrieved from word token embeddings enriched with extensive external knowledge. These anchors and prompts are used to construct prefix prompts for the signal embedding. The second component integrates high-frequency CNN features with low-frequency signal information, feeding the fused output into the pre-trained LLM.

In this work, GPT-2 is adopted as the backbone. During training, we not only learn the mapping function between inputs and outputs but also fine-tune GPT-2 using the LoRA technique [Hu *et al.*, 2021].

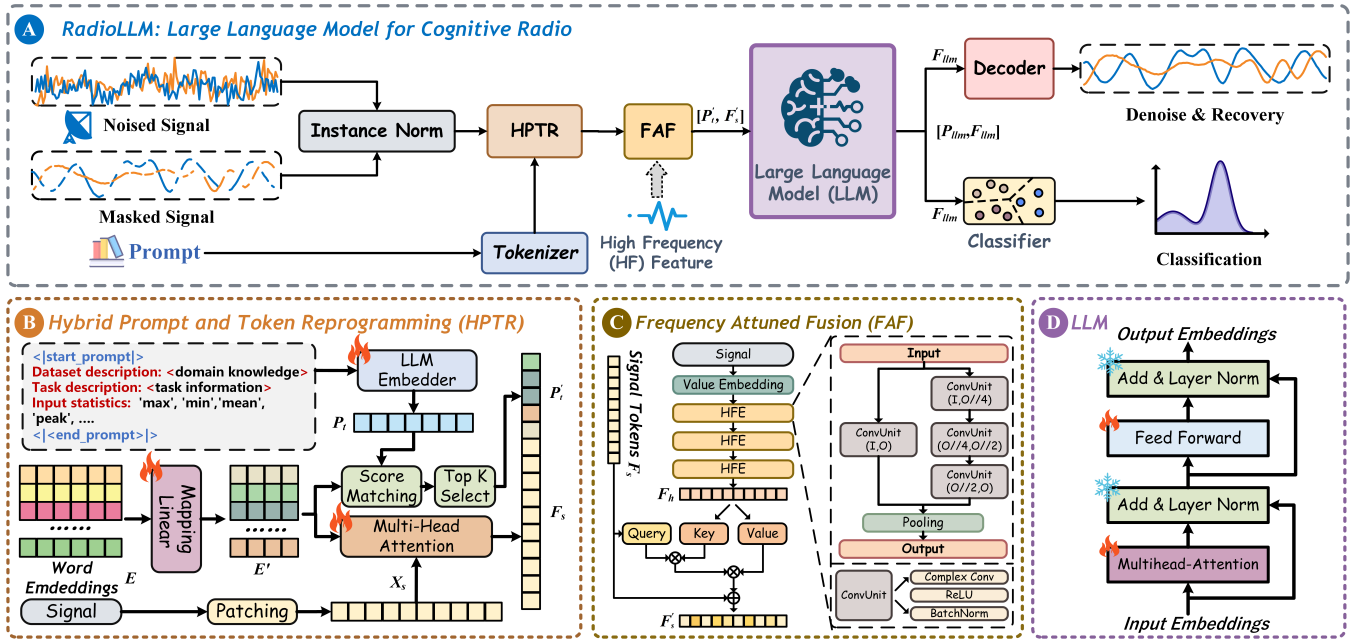


Figure 2: The model framework of RadioLLM. The input radio signal is preprocessed to generate signal embeddings  $X_s$  (A). In the HPTR stage (B),  $X_s$  is reprogrammed with semantic anchors  $E'$ , and top-K semantic anchors are selected as prefix prompt  $P'_t$ . The FAF stage (C) injects high-frequency features to address the transformer’s low-pass filtering tendency. Finally, the enhanced embeddings and prefix prompts are fed into the LLM (A&D), which outputs denoised signals  $O_s$  or classification results depending on the task.

### 3.1 Problem Statement

In cognitive radio systems, the signal received by the secondary user device is often distorted due to the effects of the wireless channel and environmental noise. The received IQ signal  $r(t) \in \mathbb{R}^{2 \times L}$  can be modeled as:

$$r(t) = h(t) * s(t) + n(t), \quad (1)$$

where  $s(t)$  is the transmitted signal,  $h(t)$  represents the channel response (e.g., path loss, multipath effects), and  $n(t)$  is the additive white Gaussian noise (AWGN). Here,  $L$  is the signal length, and 2 corresponds to the in-phase (I) and quadrature (Q) components.

The goal is to design a unified framework that can address multiple downstream tasks, including denoising, signal recovery, and classification. Let  $T$  denote the task-specific target:

- For signal reconstruction tasks (including denoising and recovery),  $T = s'(t)$ , where  $s'(t)$  represents the reconstructed signal or a task-specific attribute of the original transmitted signal.
- For classification tasks,  $T = y$ , where  $y \in \{1, 2, \dots, C\}$  is the class label associated with the signal.

To address these tasks, we aim to learn a unified model  $F(r(t); \Theta)$ , parameterized by  $\Theta$ , which maps the received signal  $r(t)$  to the target  $T$ . The unified optimization objective can be expressed as:

$$\hat{\Theta} = \arg \min_{\Theta} \mathbb{E}[\mathcal{L}(F(r(t); \Theta), T)], \quad (2)$$

where  $\mathcal{L}(\cdot, \cdot)$  is a task-specific loss function.

### 3.2 Hybrid Prompt and Token Reprogramming

Hardware prompts are widely used to inject expert knowledge into LLMs but often involve verbose, template-based structures that dilute meaningful information and increase computational cost. In contrast, pretrained software prompts encode general world knowledge but lack domain-specific relevance. To address these limitations, we propose a hybrid prompt mechanism, which combines hardware prompts with a reduced set of software prompts to achieve efficient and domain-relevant representations.

Given pretrained word token embeddings  $E \in \mathbb{R}^{V \times D}$ , where  $V$  is the vocabulary size and  $D$  is the embedding dimension, we derive a reduced set of semantic anchors  $E' \in \mathbb{R}^{V' \times D}$  ( $V' \ll V$ ) via a mapping function  $f(E)$ . For a hardware prompt  $T$ , tokenized and embedded as  $P_t \in \mathbb{R}^{L_T \times D}$ , we compute a hybrid prompt  $P'_t \in \mathbb{R}^{K \times D}$  by selecting the top- $K$  most similar embeddings from  $E'$ , formalized as:

$$P'_t[k, :] = E' \left[ \text{ArgTopK} \left( \max_{i=1}^{L_T} \gamma(P_t[i, :], E'), K \right) [k, :], \right], \quad (3)$$

where  $\gamma(\cdot)$  is the cosine similarity function defined as:

$$\gamma(P_t[i, :], E') = \frac{P_t[i, :] \cdot E'^T}{\|P_t[i, :]\| \cdot \|E'\|}. \quad (4)$$

Here,  $P'_t \in \mathbb{R}^{K \times D}$  represents the hybrid prompt constructed by selecting the top- $K$  embeddings from  $E'$ , based on the maximum cosine similarity scores over all  $L_T$  tokens in  $P_t$ .

Since LLMs are trained on textual tokens, radio signals cannot be directly understood by LLMs nor described losslessly in natural language. Therefore, it is necessary to repro-

gram the radio signal sequences into semantic tokens interpretable by the LLM. To achieve this, we leverage a multi-head cross-attention layer for the reprogramming process. Specifically, we use  $X_s$  as the query matrix and  $E'$  as the key and value matrices. The reprogramming operation for each attention head is defined as follows:

$$\text{Attention}(X_s, E', E') = \text{softmax} \left( \frac{X_s W_q (E' W_k)^T}{\sqrt{d_k}} \right) E' W_v, \quad (5)$$

where  $W_q$ ,  $W_k$ , and  $W_v$  are the learnable projection matrices for the query, key, and value, respectively, and  $d_k$  is the dimension of the key vectors. The outputs from all attention heads are concatenated and passed through a linear transformation. This linear projection maps the output of the attention layer to the LLM-compatible dimension, resulting in the signal tokens  $F_s \in \mathbb{R}^{P \times D}$ , where  $P$  is the number of patches and  $D$  is the feature dimension. These signal tokens are then fed into the LLM for further processing.

### 3.3 Frequency Attuned Fusion

Existing LLMs, based on the Transformer architecture, excel at capturing low-frequency global information through the attention mechanism but are less sensitive to high-frequency features. In contrast, CNNs naturally excel at modeling high-frequency information. Based on this understanding, we propose the FAF module to augment the signal tokens  $F_s$ , enhancing sensitivity to high-frequency information in radio signals.

The FAF module consists of three high-frequency extraction (HFE) layers, with the structure of each HFE layer shown in Figure. 2(C). Each HFE layer leverages convolution to detect local variations, ReLU to enhance non-linear features, and pooling to compress redundant information, effectively extracting high-frequency features from the input data. This design enables the network to better capture fine-grained details in the input.

The FAF module takes the raw signal  $r(t)$  as input and outputs high-frequency features  $F_h \in \mathbb{R}^{P \times D}$  after three HFE layers. Subsequently, original signal tokens are reprogrammed with the high-frequency features  $F_h$ , while also being incorporated as a supplementary component. This process yields the frequency-enhanced signal tokens  $F'_s \in \mathbb{R}^{P \times D}$ . By integrating both global low-frequency information and fine-grained high-frequency details, these enhanced tokens enable the model to achieve a more comprehensive representation of the input radio signal.

### 3.4 Output Projection

The features  $F'_s$  and  $P'_t$  are fed into the fine-tuned LLM module (Figure. 2(D)) to obtain  $F_{llm}$  and  $P_{llm}$ . After discarding the prefix  $P_{llm}$ ,  $F_{llm}$  is passed to the decoder to generate the output  $O_s \in \mathbb{R}^{2 \times L}$ . In this work, we explore two decoding strategies: a linear layer for direct mapping and a shallow Transformer decoder that uses self-attention to capture complex dependencies, yielding better reconstruction. The pretraining objective is to minimize the mean squared error (MSE) loss between  $O_s$  and the ground truth  $s'(t)$ .

## 3.5 Training Strategy

The overall pretraining pipeline of RadioLLM and its application to downstream tasks are summarized in Algorithm 1. The process begins with the configuration of hyperparameters, including the network structure, optimizer, dataset parameters, and early stopping criteria. During pretraining, most parameters of the LLM remain frozen, with only a subset updated via LoRA [Kotaru, 2023]. To compute the loss across batches from different datasets within the same epoch, a loss balancing factor  $b_i$  is introduced to mitigate the impact of differing dataset scales. Upon completion of pretraining, only the non-frozen parameters are retained to reduce storage overhead.

For downstream tasks,  $F'_s$ , extracted from the LLM output, is used as the feature representation for classification tasks. After pooling, it is fed into a linear classification head. The decoder's output  $O_s$  is directly used as the prediction for denoising and completing tasks.

---

#### Algorithm 1 RadioLLM Pretraining and Applications

---

**Input:** Unlabeled dataset  $\mathcal{D}^U = \{D_i^U\}_{i=1}^N$ , labeled dataset  $\mathcal{D} = \{D_i\}_{i=1}^N$ , balancing factors  $\{b_i\}_{i=1}^N$ , model parameters  $\Theta$ , hyperparameters (learning rate  $lr$ , batch size  $B$ , total epochs  $E$ ).

**Output:** Pretrained model parameters  $\Theta^*$ , recovery signal  $O_s$ , classification result  $Y_s$ .

- 1: **Stage 1: Pretraining RadioLLM**
  - 2: **Initialize** the parameters of  $\Theta$ .
  - 3: **for**  $e \leftarrow 1$  to  $E$  epochs **do**
  - 4:   **for** batch  $\{r(t)\}_{i=1}^B \in D_i^U$  **do**
  - 5:      $F_s, P'_t \leftarrow F_{HPTTR}(\{r(t)\}_{i=1}^B)$
  - 6:      $F'_s \leftarrow F_{FAF}(F_s)$
  - 7:      $[P_{llm}, F_{llm}] \leftarrow F_{LLM}(F'_s, P'_t)$
  - 8:      $O_s \leftarrow F_{Decoder}(F_{llm})$
  - 9:      $\mathcal{L} \leftarrow b_i \cdot \mathcal{L}_i(O_s, T)$                    ▷ Compute MSE loss
  - 10:      $\Theta \leftarrow \Theta - lr_{ssl} \nabla_{\Theta} \mathcal{L}$
  - 11:   **end for**
  - 12:   **if**  $\mathcal{L}$  does not decrease for 20 consecutive epochs **then**
  - 13:     **break**
  - 14:   **end if**
  - 15: **end for**
  - 16:  $\Theta^* \leftarrow \Theta$
  - 17: Save the non-frozen parameters of  $\Theta^*$ .
  - 18: **Stage 2: Downstream Tasks Application**
  - 19: **if** Task = RSC **then**
  - 20:   Initialize the parameters of classifier  $F_{fc}(\cdot, \Theta_{fc})$ .
  - 21:   **for** batch  $\{r(t), y\}_{i=1}^B \in D_i$  **do**
  - 22:      $Y_s \leftarrow F_{fc}(\text{Pool}(F'_s), \Theta_{fc})$
  - 23:      $\mathcal{L} \leftarrow \mathcal{L}_i(Y_s, y)$                    ▷ Compute Cross-Entropy loss
  - 24:      $\Theta_{fc} \leftarrow \Theta_{fc} - lr_{rsc} \nabla_{\Theta_{fc}} \mathcal{L}$
  - 25:   **end for**
  - 26: **else**
  - 27:   Output  $\leftarrow O_s$
  - 28: **end if**
-



## 4 Experiments

### 4.1 Data

We used six publicly available datasets (RML2016a, RML2016b [O’Shea and West, 2016], RML2016c [O’Shea *et al.*, 2016], RML2018a [O’Shea *et al.*, 2018], ADS-B [?], and Wi-Fi [Sankhe *et al.*, 2019]) consolidated into a unified dataset. To prevent data leakage in downstream tasks, the data was split into training, validation, and test sets in a ratio of 8:1:1. For pretraining, high signal-to-noise ratio (SNR) signals ( $\text{SNR} \geq 14$  dB) from the RML datasets were selected, while all signals from ADS-B and Wi-Fi datasets were included.

### 4.2 Implementation Details

During the training process, we conducted all experiments, including pretraining, comparisons, and ablations, on two A800 Ubuntu servers using the PyTorch 2.3.0 framework. The AdamW optimizer (weight decay =  $5 \times 10^{-3}$ ) was employed with an initial learning rate of  $5 \times 10^{-5}$ . A linear warmup and decay schedule was applied during the pretraining phase, with the warmup phase covering 10% of the total training epochs. The training process was capped at 50 epochs, and the learning rate was halved if the validation loss stagnated for 5 consecutive epochs. Additionally, early stopping was triggered if validation loss did not improve for 20 consecutive epochs.

For downstream tasks like classification and denoising, a cosine annealing learning rate schedule was employed, starting with an initial learning rate of  $5 \times 10^{-5}$ . All experiments were conducted under uniform settings to maintain fairness across methods and tasks. Inference time was measured in seconds per batch, with the batch size fixed at 128.

### 4.3 Evaluation Metrics

To meet practical requirements, we employed widely used metrics for quantitative assessment, including Overall Accuracy (OA), Cohen’s Kappa coefficient (Kappa), and Structural Similarity Index Measure (SSIM). OA and Kappa were utilized to evaluate classification performance, measuring overall accuracy and agreement beyond chance, respectively. SSIM was used to assess the structural similarity between predicted and ground truth signals, providing a perceptually aligned evaluation of reconstruction quality.

### 4.4 Comparison with RSC methods

We evaluated our proposed method against a range of RSC approaches, including supervised models such as HCGDNN [Chang *et al.*, 2022], PETCGDNN [Zhang *et al.*, 2021b], MCLDNN [Xu *et al.*, 2020], ICMACNET [Hermawan *et al.*, 2020], CVCNN [Wang *et al.*, 2021], SFS-SEI [Tao *et al.*, 2023], and CVSRN [Han *et al.*, 2024], as well as unsupervised methods like SemiAMC [Liu *et al.*, 2021] and TC-SSAMR [Kong *et al.*, 2023b]. For methods lacking publicly available code, we reconstructed their networks based on descriptions in their respective papers and retrained them. For other methods, we used pretrained models or retrained them under identical experimental settings to ensure fair comparisons.

Experiments were conducted on several datasets across different configurations. We evaluated the RML2016a, RML2016b, and RML2016c datasets under both 50-shot and 100-shot settings, while the RML2018a Wi-Fi dataset was tested with a 100-shot setting. For the ADS-B dataset, 10% of the total data was used for fine-tuning due to its limited size. Full details of the experimental setups, including preprocessing, training, and evaluation protocols, are provided in the Appendix. As shown in Table 1, RadioLLM, pre-trained on large-scale data, consistently demonstrated superior performance across multiple datasets. On RML2016a, it outperformed TcssAMR in both 50-shot and 100-shot settings, showcasing the advantages of pre-training for feature extraction. However, Figure 3 reveals challenges with distinguishing similar modulation schemes like 16-QAM and 64-QAM, as well as noise-prone signals such as WBFM and AM-DSB.

On RML2016b, RadioLLM slightly surpassed SemiAMC in the 50-shot setting and maintained a clear edge over TcssAMR in the 100-shot setting, particularly excelling in low-noise environments. For the imbalanced RML2016c dataset, it demonstrated effective transfer learning by reducing misclassifications among similar modulation types, notably outperforming TcssAMR in both settings.

RadioLLM also outperformed competing models on more complex datasets. On RML2018a, it managed increased task complexity better than MCLDNN, while on the Wi-Fi dataset, it achieved the highest performance among all methods tested, effectively handling intricate signal patterns. As shown in Figure 3, for the RML2018a dataset, misclassifications among similar modulation types, such as 8PSK and BPSK, were infrequent. This highlights the effectiveness of transfer learning in distinguishing between closely related signal types. On the ADS-B dataset, while RadioLLM did not achieve the best performance, its results were still acceptable. We evaluated the model’s generalization ability on an unseen dataset, RML2022 [Sathyanarayanan *et al.*, 2023b]. The detailed experimental results are provided in the Appendix.

In conclusion, RadioLLM demonstrates exceptional adaptability and generalization across a wide range of RSC tasks. On most datasets, RadioLLM achieved state-of-the-art performance, showcasing its ability to handle diverse and complex signal classification challenges. Its robust feature extraction and versatility make it a reliable solution for tasks requiring both precision and adaptability.

### 4.5 Comparison with Denoise methods

We evaluated our proposed method against traditional and deep learning-based denoising models across three datasets. For models without publicly available implementations, we reconstructed and retrained them following their published methodologies. Pretrained models were used when available; otherwise, all methods were retrained under identical conditions for fair comparisons (details provided in the Appendix). As shown in Table 2, RadioLLM achieves the highest SSIM across all datasets (0.987, 0.984, 0.986), underscoring its superior ability to preserve structural similarity. DNCNet [Du *et al.*, 2022] demonstrates comparable performance, with SSIM values trailing marginally by 0.001–0.003, indicating its competitiveness. In contrast, the SGFilter [Schafer, 2011] falls

Methods	RML2016a				RML2016b				RML2016c				RML2018a		Wi-Fi		ADS-B	
	50-shot		100-shot		50-shot		100-shot		50-shot		100-shot		100-shot		100-shot		10%	
	OA(%)	Kappa	OA(%)	Kappa	OA(%)	Kappa	OA(%)	Kappa	OA(%)	Kappa	OA(%)	Kappa	OA(%)	Kappa	OA(%)	Kappa	OA(%)	Kappa
HCGDNN	54.58	0.5004	54.30	0.4973	54.38	0.4931	55.30	0.5033	63.59	0.5919	64.71	0.6066	16.98	0.1337	15.67	0.1004	44.66	0.4434
PETCGDNN	48.05	0.4286	51.09	0.4620	48.94	0.4326	50.91	0.4546	61.65	0.5708	61.71	0.5724	30.98	0.2798	<u>34.59</u>	<u>0.3023</u>	97.47	0.9746
MCLDNN	39.65	0.3362	52.84	0.4812	39.52	0.3280	52.45	0.4716	62.91	0.5843	65.53	0.6159	<u>52.03</u>	<u>0.4994</u>	19.41	0.1403	65.12	0.6493
ICAMCNET	52.55	0.4780	53.55	0.4891	52.30	0.4700	53.43	0.4825	61.98	0.5742	63.17	0.5892	31.48	0.2850	11.34	0.0543	<b>99.09</b>	<b>0.9908</b>
CVCNN	52.13	0.4735	54.15	0.4957	52.03	0.4669	54.06	0.4896	63.78	0.5939	65.37	0.6112	32.34	0.2940	11.44	0.0553	97.49	0.9747
SFS-SEI	51.62	0.4678	54.13	0.4954	51.93	0.4659	54.17	0.4907	62.49	0.5823	65.37	0.6124	31.86	0.2890	11.45	0.0555	<u>97.50</u>	<u>0.9749</u>
CVSRN	47.62	0.4238	47.56	0.4232	49.65	0.4405	51.50	0.4611	<u>64.45</u>	<u>0.6012</u>	61.76	0.5726	32.05	0.2910	11.72	0.0583	94.55	0.9452
TessAMR	<u>55.01</u>	<u>0.5052</u>	<u>56.53</u>	<u>0.5218</u>	<u>55.02</u>	<u>0.5002</u>	55.98	0.5109	63.93	0.5964	<u>66.21</u>	<u>0.6224</u>	44.96	0.4257	32.86	0.2873	61.89	0.6177
SemiAMC	54.47	0.4991	55.32	0.5076	54.64	0.4960	<u>56.17</u>	<u>0.5129</u>	63.10	0.5869	64.62	0.6056	42.05	0.3953	29.36	0.2502	70.42	0.7034
RadioLLM	<b>56.46</b>	<b>0.5211</b>	<b>58.10</b>	<b>0.5391</b>	<b>56.11</b>	<b>0.5123</b>	<b>58.35</b>	<b>0.5372</b>	<b>66.66</b>	<b>0.6275</b>	<b>68.19</b>	<b>0.6441</b>	<b>54.21</b>	<b>0.5222</b>	<b>35.41</b>	<b>0.3110</b>	90.58	0.9054

Table 1: Comparison of Methods on Classification Tasks. **BOLD** indicates the best performance, and UNDERLINED indicates the second-best performance.

Method	RML2016a	RML2016b	RML2016c
SGFilter	0.979	0.974	0.978
DNCNet	0.986	0.987	0.986
RadioLLM	0.987	0.984	0.986

Table 2: SSIM values for different models across datasets.

short (0.979–0.978), reflecting the limitations of traditional methods compared to deep learning approaches. The slightly lower performance observed for all models on RML2016b may be attributed to unique noise characteristics or increased data complexity in this dataset.

#### 4.6 Ablation Studies

To thoroughly evaluate the effectiveness of the proposed HTRP and FAF modules, a series of ablation experiments were conducted. These experiments systematically explored the contribution of each module to the overall model performance, offering deeper insights into their individual and combined impacts. Unless explicitly mentioned otherwise, all ablation studies were performed on the RML2016a dataset, using the experimental setup outlined in Section 4.2. The results are summarized in Table 3. The baseline model, which

HTRP	FAF	OA (%)	Kappa	SSIM
✗	✗	55.39	0.5097	0.9839
✓	✗	57.08	0.5283	0.9873
✗	✓	57.25	0.5306	0.9837
✓	✓	58.10	0.5391	0.9819

Table 3: Ablation study results for the HTRP and FAF modules.

excluded both HTRP and FAF modules, achieved 55.39% OA, a Kappa of 0.5097, and a SSIM of 0.9839. Introducing the HTRP module alone improved the OA to 57.08%, the Kappa to 0.5283, and the SSIM to 0.9873. This improvement demonstrates the module’s capacity to inject domain-specific knowledge, thereby enhancing the model’s ability to identify relevant features.

Similarly, incorporating the FAF module independently yielded a slightly higher OA of 57.25% and a Kappa of 0.5306, while maintaining an SSIM of 0.9837. This suggests that FAF excels at extracting fine-grained, high-frequency features, contributing to a more detailed signal representation.

When both modules were combined, the model achieved the highest performance across all metrics. Specifically, the OA increased to 58.10%, and the Kappa improved to 0.5391, although the SSIM saw a marginal decrease to 0.9819. These results highlight the complementary strengths of the two modules: HTRP enhances domain-relevant feature extraction, while FAF focuses on capturing intricate details. Together, they create a synergistic effect, integrating global low-frequency and fine-grained high-frequency features to improve classification accuracy and robustness.

#### 4.7 Parameter Sensitivity Analysis

To assess the impact of key parameters on our framework’s performance, we conducted a sensitivity analysis focusing on Top-K ( $K$ ) selection, Decoder usage, and LLM choice. The experiments were performed on the RML2016a dataset under a consistent 100-shot learning setting to ensure fair comparisons. The results and observations for each parameter are detailed below.

##### Top-K ( $K$ )

While increasing  $K$  can improve metrics such as OA and Kappa by capturing richer information, it also increases computational load, leading to longer inference times. This study analyzes the sensitivity of OA, Kappa, and inference time (seconds per batch) to variations in  $K$ , highlighting the trade-offs between performance and efficiency. As depicted in Figure 4, the results demonstrate that  $K = 7$  represents the optimal balance, achieving the highest performance (OA and Kappa) with a reasonable computational cost in terms of inference time.

##### Decoder Usage

To further investigate the impact of the decoder, we conducted experiments by removing it and compared the model’s performance across tasks. The results indicate that removing the decoder causes a slight performance decline. Specifically,

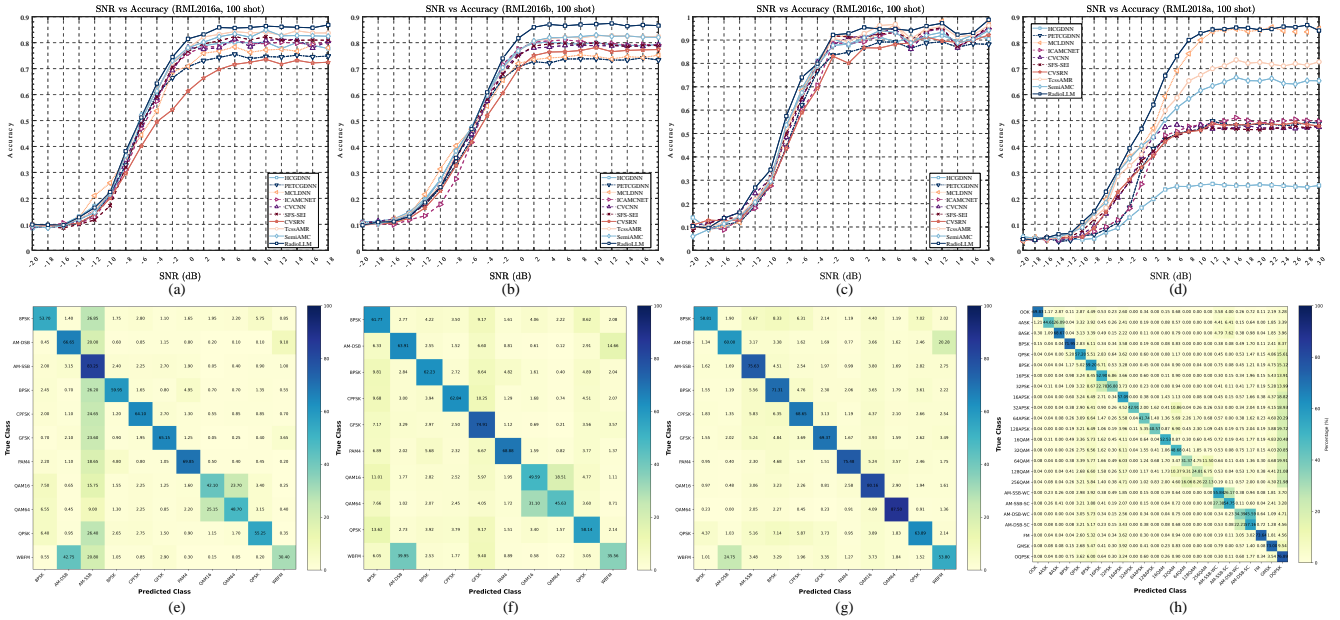


Figure 3: Performance analysis of RadioLLM across SNR levels and confusion matrices on multiple datasets. Specifically, (a-d) show the OA of RadioLLM compared to other models under different SNR conditions on datasets RML2016a, RML2016b, RML2016c, and RML2018a, respectively. Meanwhile, (e-h) present the confusion matrices of RadioLLM on the corresponding datasets, providing a detailed view of its classification performance for various modulation classes, highlighting both strengths and potential areas of misclassification.

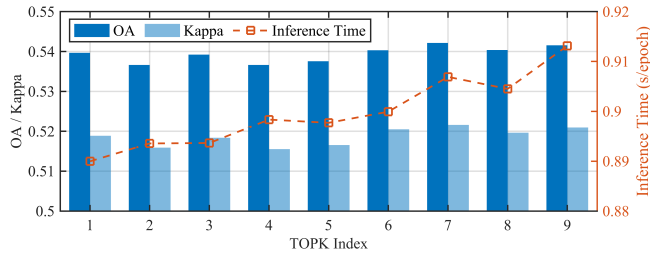


Figure 4: Performance Comparison Across Different K Values

OA dropped from 0.58312 to 0.57413, reflecting a decrease of 0.899%, while the Kappa coefficient decreased from 0.5419 to 0.532, a reduction of 0.0099.

These findings underscore the importance of the decoder in enhancing classification accuracy and consistency. By refining the model’s contextual understanding and improving representation quality, the decoder significantly contributes to better task performance.

### LLM Choice

The choice of LLM directly impacts the performance and efficiency of the RadioLLM framework. We evaluated BERT, GPT-2, and LLaMA3 based on OA, Kappa, and Inference Time (seconds per batch). The results, shown in Table 4, highlight the trade-offs between classification performance and computational cost.

As shown in Table 4, LLaMA3 achieves the highest OA and Kappa but has a slightly higher inference time. GPT-2 offers a balance between performance and efficiency, with competitive accuracy and the lowest inference time. BERT,

LLM	OA (%)	Kappa	Inference Time
BERT	57.53	0.5332	1.7519
GPT-2	58.10	0.5391	0.9069
LLaMA3	58.67	0.5480	0.9319

Table 4: Performance Comparison Across Different LLMs

while fastest to deploy in some contexts, has lower accuracy and the longest inference time, making it less ideal for large-scale deployments.

## 5 Conclusion

This paper introduces RadioLLM, an innovative framework aimed at advancing CRT by seamlessly integrating radio signal processing with LLMs. The proposed HPTR mechanism effectively bridges the gap between radio signals and LLMs by combining hardware and semantic software prompts, enabling efficient and domain-specific representations. Complementing this, the FAF module enhances the framework’s ability to capture fine-grained high-frequency features, which are crucial for handling complex signal environments in CRT. Extensive experiments across diverse tasks validate RadioLLM’s effectiveness in addressing prominent challenges in CRT, such as noisy conditions, imbalanced datasets, and intricate signal patterns. These contributions establish RadioLLM as a robust and adaptable solution, paving the way for future advancements in cognitive radio systems.

## References

- [Bai *et al.*, 2022] Jiawang Bai, Li Yuan, Shu-Tao Xia, Shuicheng Yan, Zhifeng Li, and Wei Liu. Improving vision transformers by revisiting high-frequency components. pages 1–18, 2022.
- [Cao *et al.*, 2024] Defu Cao, Furong Jia, Sercan O Arik, Tomas Pfister, Yixiang Zheng, Wen Ye, and Yan Liu. TEMPO: Prompt-based generative pre-trained transformer for time series forecasting. In *The Twelfth International Conference on Learning Representations*, 2024.
- [Chang *et al.*, 2022] Shuo Chang, Ruiyun Zhang, Kejia Ji, Sai Huang, and Zhiyong Feng. A hierarchical classification head based convolutional gated deep neural network for automatic modulation classification. *IEEE Transactions on Wireless Communications*, 21(10):8713–8728, 2022.
- [Chen *et al.*, 2024] Shuai Chen, Zhixi Feng, Shuyuan Yang, Yue Ma, Jun Liu, and Zhuoyue Qi. A generative self-supervised framework for cognitive radio leveraging time-frequency features and attention-based fusion. *IEEE Transactions on Wireless Communications*, 2024.
- [Du *et al.*, 2022] Mingyang Du, Ping Zhong, Xiaohao Cai, and Daping Bi. Dncnet: Deep radar signal denoising and recognition. *IEEE Transactions on Aerospace and Electronic Systems*, 58(4):3549–3562, 2022.
- [Feng *et al.*, 2024] Zhixi Feng, Shuai Chen, Yue Ma, Yachen Gao, and Shuyuan Yang. Learning temporal–spectral feature fusion representation for radio signal classification. *IEEE Transactions on Industrial Informatics*, pages 1–10, 2024.
- [Haider *et al.*, 2015] Fourat Haider, Cheng-Xiang Wang, Harald Haas, Erol Hepsaydir, Xiaohu Ge, and Dongfeng Yuan. Spectral and energy efficiency analysis for cognitive radio networks. *IEEE Transactions on Wireless Communications*, 14(6):2969–2980, 2015.
- [Han *et al.*, 2024] Guangjie Han, Zhengwei Xu, Hongbo Zhu, Yunlu Ge, and Jinlin Peng. A two-stage model based on a complex-valued separate residual network for cross-domain iiot devices identification. *IEEE Transactions on Industrial Informatics*, 20(2):2589–2599, 2024.
- [Hermawan *et al.*, 2020] Ade Pitra Hermawan, Rizki Rivai Ginanjar, Dong-Seong Kim, and Jae-Min Lee. Cnn-based automatic modulation classification for beyond 5g communications. *IEEE Communications Letters*, 24(5):1038–1041, 2020.
- [Hu *et al.*, 2021] Edward J Hu, Yelong Shen, Phillip Wallis, Zeyuan Allen-Zhu, Yuanzhi Li, Shean Wang, Lu Wang, and Weizhu Chen. Lora: Low-rank adaptation of large language models. *arXiv preprint arXiv:2106.09685*, 2021.
- [Jin *et al.*, 2024] Ming Jin, Shiyu Wang, Lintao Ma, Zhixuan Chu, James Y. Zhang, Xiaoming Shi, Pin-Yu Chen, Yuxuan Liang, Yuan-Fang Li, Shirui Pan, and Qingsong Wen. Time-LLM: Time series forecasting by reprogramming large language models. In *The Twelfth International Conference on Learning Representations*, 2024.
- [Kaushal *et al.*, 2016] Gautam Kaushal, Amanpreet Singh, and VK Jain. Better approach for denoising eeg signals. In *2016 5th International Conference on Wireless Networks and Embedded Systems (WECON)*, pages 1–3. IEEE, 2016.
- [Ke and Vikalo, 2021] Ziqi Ke and Haris Vikalo. Real-time radio technology and modulation classification via an lstm auto-encoder. *IEEE Transactions on Wireless Communications*, 21(1):370–382, 2021.
- [Kong *et al.*, 2023a] Weisi Kong, Xun Jiao, Yuhua Xu, Bolin Zhang, and Qinghai Yang. A transformer-based contrastive semi-supervised learning framework for automatic modulation recognition. *IEEE Transactions on Cognitive Communications and Networking*, 9(4):950–962, 2023.
- [Kong *et al.*, 2023b] Weisi Kong, Xun Jiao, Yuhua Xu, Bolin Zhang, and Qinghai Yang. A transformer-based contrastive semi-supervised learning framework for automatic modulation recognition. *IEEE Transactions on Cognitive Communications and Networking*, 9(4):950–962, 2023.
- [Kotaru, 2023] Manikanta Kotaru. Adapting foundation models for information synthesis of wireless communication specifications. *arXiv preprint arXiv:2308.04033*, 2023.
- [Liu *et al.*, 2021] Dongxin Liu, Peng Wang, Tianshi Wang, and Tarek Abdelzaher. Self-contrastive learning based semi-supervised radio modulation classification. In *MILCOM 2021 - 2021 IEEE Military Communications Conference (MILCOM)*, pages 777–782, 2021.
- [Nahum *et al.*, 2023] Cleverson Veloso Nahum, Victor Hugo L Lopes, Ryan M Dreifuerst, Pedro Batista, Ilan Correa, Kleber Vieira Cardoso, Aldebaro Klautau, and Robert W Heath. Intent-aware radio resource scheduling in a ran slicing scenario using reinforcement learning. *IEEE Transactions on Wireless Communications*, 23(3):2253–2267, 2023.
- [O’shea and West, 2016] Timothy J O’shea and Nathan West. Radio machine learning dataset generation with gnu radio. In *Proceedings of the GNU radio conference*, volume 1, 2016.
- [O’Shea *et al.*, 2016] Timothy J O’Shea, Johnathan Corgan, and T Charles Clancy. Convolutional radio modulation recognition networks. In *Engineering Applications of Neural Networks: 17th International Conference, EANN 2016, Aberdeen, UK, September 2-5, 2016, Proceedings 17*, pages 213–226. Springer, 2016.
- [O’Shea *et al.*, 2018] Timothy James O’Shea, Tamoghna Roy, and T Charles Clancy. Over-the-air deep learning based radio signal classification. *IEEE Journal of Selected Topics in Signal Processing*, 12(1):168–179, 2018.
- [Pan *et al.*, 2024] Zijie Pan, Yushan Jiang, Sahil Garg, Anderson Schneider, Yuriy Nevmyvaka, and Dongjin Song. S2ip-llm: Semantic space informed prompt learning with llm for time series forecasting. In *Forty-first International Conference on Machine Learning*, 2024.

- [Sankhe *et al.*, 2019] Kunal Sankhe, Mauro Belgiovine, Fan Zhou, Shamnaz Riyaz, Stratis Ioannidis, and Kaushik Chowdhury. Oracle: Optimized radio classification through convolutional neural networks. In *IEEE INFOCOM 2019-IEEE Conference on Computer Communications*, pages 370–378. IEEE, 2019.
- [Sathyanarayanan *et al.*, 2023a] Venkatesh Sathyanarayanan, Peter Gerstoft, and Aly El Gamal. Rml22: Realistic dataset generation for wireless modulation classification. *IEEE Transactions on Wireless Communications*, 22(11):7663–7675, 2023.
- [Sathyanarayanan *et al.*, 2023b] Venkatesh Sathyanarayanan, Peter Gerstoft, and Aly El Gamal. Rml22: Realistic dataset generation for wireless modulation classification. *IEEE Transactions on Wireless Communications*, 22(11):7663–7675, 2023.
- [Schafer, 2011] Ronald W Schafer. What is a savitzky-golay filter?[lecture notes]. *IEEE Signal processing magazine*, 28(4):111–117, 2011.
- [Shao *et al.*, 2024] Jiawei Shao, Jingwen Tong, Qiong Wu, Wei Guo, Zijian Li, Zehong Lin, and Jun Zhang. Wireless-llm: Empowering large language models towards wireless intelligence. *Journal of Communications and Information Networks*, 9(2):99–112, 2024.
- [Si *et al.*, 2022] Chenyang Si, Weihao Yu, Pan Zhou, Yichen Zhou, Xinchao Wang, and Shuicheng Yan. Inception transformer. *Advances in Neural Information Processing Systems*, 35:23495–23509, 2022.
- [Tao *et al.*, 2023] Mengyuan Tao, Xue Fu, Yun Lin, Yu Wang, Zhisheng Yao, Shengnan Shi, and Guan Gui. Resource-constrained specific emitter identification using end-to-end sparse feature selection. In *GLOBECOM 2023 - 2023 IEEE Global Communications Conference*, pages 6067–6072, 2023.
- [Wang *et al.*, 2021] Yu Wang, Guan Gui, Haris Gacanin, Tomoaki Ohtsuki, Octavia A. Dobre, and H. Vincent Poor. An efficient specific emitter identification method based on complex-valued neural networks and network compression. *IEEE Journal on Selected Areas in Communications*, 39(8):2305–2317, 2021.
- [Xiao *et al.*, 2024] Chenghong Xiao, Shuyuan Yang, Zhixi Feng, and Licheng Jiao. Mclhn: Towards automatic modulation classification via masked contrastive learning with hard negatives. *IEEE Transactions on Wireless Communications*, 2024.
- [Xie *et al.*, 2024] Huiqiang Xie, Zhijin Qin, Xiaoming Tao, and Zhu Han. Toward intelligent communications: Large model empowered semantic communications. *IEEE Communications Magazine*, pages 1–7, 2024.
- [Xu *et al.*, 2020] Jialang Xu, Chunbo Luo, Gerard Parr, and Yang Luo. A spatiotemporal multi-channel learning framework for automatic modulation recognition. *IEEE Wireless Communications Letters*, 9(10):1629–1632, 2020.
- [Zhang *et al.*, 2021a] Fuxin Zhang, Chunbo Luo, Jialang Xu, and Yang Luo. An efficient deep learning model for automatic modulation recognition based on parameter estimation and transformation. *IEEE Communications Letters*, 25(10):3287–3290, 2021.
- [Zhang *et al.*, 2021b] Fuxin Zhang, Chunbo Luo, Jialang Xu, and Yang Luo. An efficient deep learning model for automatic modulation recognition based on parameter estimation and transformation. *IEEE Communications Letters*, 25(10):3287–3290, 2021.

## A Visualization

### Signal Denoise

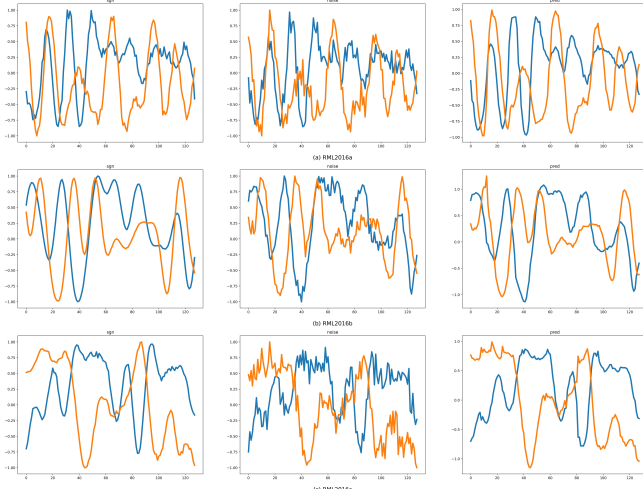


Figure 5: Results of signal denoising. The figure illustrates the performance of denoising models on noisy input signals, comparing reconstructed outputs with their corresponding clean signals.

### Confusion Matrix

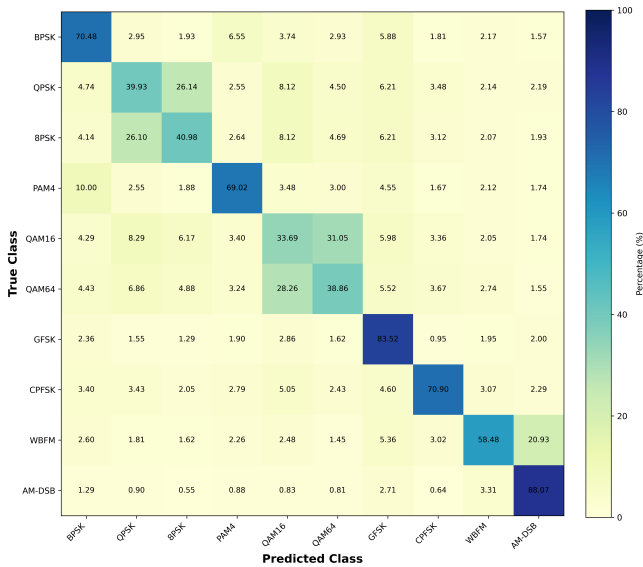


Figure 6: Confusion Matrix on RML2022 Dataset Across All SNR Levels

## B Dataset Details

To validate the effectiveness of the proposed method, extensive experiments were conducted on seven publicly available datasets: RadioML2016.10a, RadioML2016.10b, RML2016.04c, RML2018.01a, the ADS-B dataset collected in real-world scenarios, and the Wi-Fi dataset.

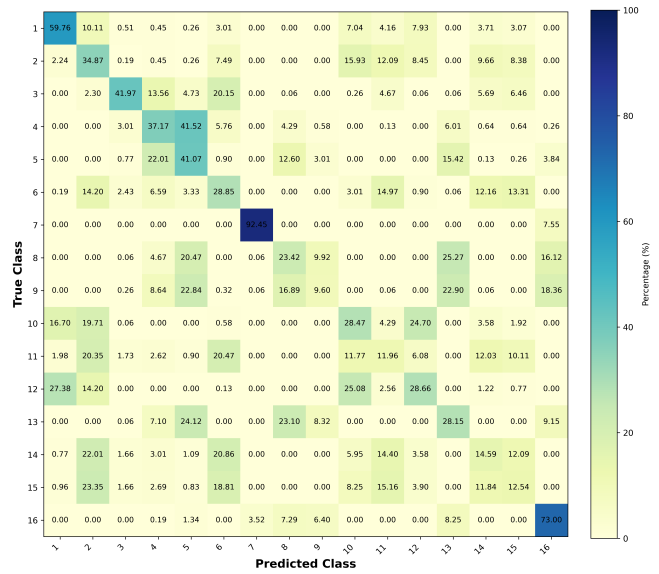


Figure 7: Confusion Matrix on Wi-Fi Dataset

For simplicity, these datasets are referred to as RML16a, RML16b, RML16c, RML18a, ADS-B, and Wi-Fi, respectively, throughout this paper.

**RML2016a:** The RML2016.10a dataset consists of 220,000 modulated signals generated under simulated interference conditions, including Carrier Frequency Offset and Additive White Gaussian Noise. Each signal comprises 128 complex-valued in-phase and quadrature sample points. This dataset includes a diverse range of modulation schemes, covering three analog modulation types—Wideband Frequency Modulation (WBFM), Amplitude Modulation Single Sideband (AM-SSB), and Amplitude Modulation Double Sideband (AM-DSB)—as well as eight digital modulation types: Continuous Phase Frequency Shift Keying (CPFSK), Binary Phase Shift Keying (BPSK), 8-Phase Shift Keying (8PSK), Gaussian Frequency Shift Keying (GFSK), 16-Quadrature Amplitude Modulation (16-QAM), 64-Quadrature Amplitude Modulation (64-QAM), 4-Pulse Amplitude Modulation (4PAM), and Quadrature Phase Shift Keying (QPSK).

**RML2016b:** The RML2016.10b dataset contains 1.2 million modulated signals, encompassing the same modulation schemes as RMLa, with the exception of AM-SSB. Each signal also consists of 128 complex-valued I/Q samples.

**RML2016c:** The RML2016.10c dataset comprises 162,060 modulated signals with the same modulation categories as RMLa. Each signal similarly contains 128 I/Q data points.

**RML2018a:** The RML2018.01a dataset is a large-scale benchmark dataset for signal modulation classification. It contains 2,555,904 signal samples representing 24 modulation types (OOK, BPSK, QPSK, 16QAM, etc.) across 26 SNR levels ranging from -20 dB to 30 dB (step size: 2 dB). Each signal sample consists of 1024 IQ data points (I for in-phase, Q for quadrature), with 4,096 samples per modulation type at each SNR level, providing a balanced and diverse dataset for training and evaluating modulation classification



models.

**RML2022:** The RML2022 dataset consists of 420,000 modulated signal samples, encompassing 8 types of digital modulation—8PSK, BPSK, CPFSK, GFSK, 4PAM, 16QAM, 64QAM, and QPSK—as well as 2 types of analog modulation: AM-DSB and WBFM. The dataset covers a Signal-to-Noise Ratio (SNR) range from -20 dB to 20 dB, with increments of 2 dB between levels.

**Wi-Fi:** The Wi-Fi dataset, as reported in [Sankhe *et al.*, 2019], contains over-the-air transmissions captured using 16 USRP X310 transmitters at a fixed distance of 2 feet between the transmitter and receiver. The raw signals were processed into sequences of 128 complex-valued I/Q samples to align with the format of other datasets.

**ADS-B:** The ADS-B dataset includes 63,105 Automatic Dependent Surveillance-Broadcast signals captured in open, real-world environments. Each signal is sampled at a rate of 50 MHz, containing 3,000 sampling points. This dataset spans 198 distinct signal classes.

## C Experimental Details

### C.1 Data Organization

The data partitioning strategy for the datasets RML2016a, RML2016b, RML2016c, RML2018a, RML2022, Wi-Fi, and ADS-B is as follows:

Selection of Experimental Data: The datasets are first filtered by selecting proportions of the original data:

- RML2016a: 100% of the dataset is used.
- RML2016b: 100% of the dataset is used.
- RML2016c: 100% of the dataset is used.
- RML2018a: 25% of the dataset is used.
- RML2022: 25% of the dataset is used.
- Wi-Fi: 10% of the dataset is used.
- ADS-B: 100% of the dataset is used.

Data Splitting: After selection, the data is split into training (80%), validation (10%), and test (10%) sets.

Pretraining Stage:

- For the RML datasets (RML2016a, RML2016b, RML2018a), only training samples with  $\text{SNR} \geq 14$  dB are used for pretraining.
- For the Wi-Fi and ADS-B datasets, all training samples are used for pretraining.

Fine-Tuning Stage: For fine-tuning, a limited number of samples are selected from the training set:

- For RML2016a, RML2016b, and RML2016c 50 or 100 samples per class per SNR are chosen from the training set.
- For the RML2018a, RML2022 and Wi-Fi dataset, 100 samples per class are selected from the training set.
- For the ADS-B dataset, 10% of the training set is used for fine-tuning.

Denoise Task: For the denoising task, high-SNR samples ( $\text{SNR} \geq 14$  dB) from the RML series, Wi-Fi, and ADS-B datasets were artificially augmented with controlled noise to simulate noisy data. The denoising models processed these inputs, and their outputs were evaluated against the clean samples using the SSIM metric to ensure a standardized and objective assessment.

### C.2 Data Augmentation

#### Phase Rotation

Phase rotation is performed by rotating the phase of the original signal. The process can be mathematically described as:

$$s'(t) = s(t) \cdot e^{j\theta}, \quad (6)$$

where  $s(t)$  is the original signal,  $\theta$  is the rotation angle,  $j = \sqrt{-1}$ , and  $s'(t)$  is the phase-rotated signal. The angle  $\theta$  is typically chosen randomly from the interval  $[0, 2\pi)$ .

#### Signal Reverse

Signal reverse enhances the signal by flipping it along the time axis. The process is defined as:

$$s'(t) = s(-t), \quad (7)$$

where  $s(t)$  is the original signal, and  $s'(t)$  is the reversed signal. For discrete signals, the operation is expressed as:

$$s'[n] = s[N - 1 - n], \quad (8)$$

where  $N$  is the total length of the signal, and  $n$  is the discrete time index.

#### Time Warp

Time warping is a method to enhance signals by altering their temporal dynamics through nonlinear time axis transformations. The process is mathematically described as:

$$s'(t) = s(\phi(t)), \quad (9)$$

where  $s(t)$  is the original signal,  $\phi(t)$  is the time warping function, and  $s'(t)$  is the time-warped signal. The warping function  $\phi(t)$  must satisfy:

- $\phi'(t) > 0$  (monotonicity),
- $\phi(t) \in [0, T]$ , where  $T$  is the total duration of the signal.

For discrete signals, the time warping operation is expressed as:

$$s'[n] = s[\phi(n)], \quad (10)$$

where  $\phi(n)$  is the discrete time warping function.

### C.3 Metrics

This section outlines the metrics used to evaluate the denoising and classification tasks. For the classification task, we utilize Overall Accuracy (OA) and Cohen’s Kappa coefficient (Kappa), while the Structural Similarity Index Measure (SSIM) is employed for the denoising and masking task.

Dataset	Selection Proportion	Train:Val:Test	Pretraining Data	Fine-Tuning Data
<b>RML16a</b>	100%	80% : 10% : 10%	SNR $\geq$ 14 dB <sup>(a)</sup>	50 or 100 samples/class/SNR <sup>(c)</sup>
<b>RML16b</b>	100%	80% : 10% : 10%	SNR $\geq$ 14 dB <sup>(a)</sup>	50 or 100 samples/class/SNR <sup>(c)</sup>
<b>RML16c</b>	100%	80% : 10% : 10%	None	50 or 100 samples/class/SNR <sup>(c)</sup>
<b>RML18a</b>	25%	80% : 10% : 10%	SNR $\geq$ 14 dB <sup>(a)</sup>	100 samples/class/SNR <sup>(c)</sup>
<b>Wi-Fi</b>	10%	80% : 10% : 10%	5% training data <sup>(b)</sup>	100 samples/class <sup>(c)</sup>
<b>ADS-B</b>	100%	80% : 10% : 10%	100% training data	10% of training data <sup>(d)</sup>

<sup>(a)</sup> For RML datasets, only training data with SNR  $>$  14 dB is used in the pretraining phase.

<sup>(b)</sup> For Wi-Fi datasets, all training data are used in the pretraining phase.

<sup>(c)</sup> In the fine-tuning phase, 50 or 100 samples are selected per class per SNR for RML datasets and per class for Wi-Fi.

<sup>(d)</sup> For ADS-B, 10% of the training data is used for fine-tuning, while all validation and test data are used.

Table 5: Dataset Selection and Splitting Strategy

### Overall Accuracy (OA)

Overall Accuracy (OA) is a widely used metric in classification tasks to measure the proportion of correctly classified samples. It is defined as:

$$OA = \frac{\sum_{i=1}^k n_{ii}}{N},$$

where:  $n_{ii}$  is the number of correctly classified samples for class  $i$ ,  $k$  is the total number of classes,  $N$  is the total number of samples.

OA ranges from 0 to 1, where a higher value indicates better classification performance.

### Cohen’s Kappa Coefficient (Kappa)

Cohen’s Kappa coefficient is a statistical measure of inter-rater agreement or classification reliability. It accounts for the possibility of agreement occurring by chance. Kappa is defined as:

$$Kappa = \frac{OA - PE}{1 - PE},$$

where: OA is the observed accuracy (as defined above), PE is the expected agreement by chance, calculated as:

$$PE = \sum_{i=1}^k \left( \frac{\sum_{j=1}^k n_{ij} \cdot \sum_{j=1}^k n_{ji}}{N^2} \right),$$

where  $n_{ij}$  is the number of samples classified as class  $j$  when their true label is class  $i$ .

The value of Kappa ranges from  $-1$  to  $1$ , where Kappa =  $1$  indicates perfect agreement, Kappa =  $0$  indicates no agreement beyond chance, Kappa  $<$   $0$  indicates disagreement worse than chance.

### Structural Similarity Index (SSIM)

The Structural Similarity Index (SSIM) is a perceptual metric used to measure the similarity between two images. It is particularly designed to evaluate the quality of denoised or reconstructed images by comparing them with their original counterparts.

The SSIM between two signals,  $x$  and  $y$ , is defined as:

$$SSIM(x, y) = \frac{(2\mu_x\mu_y + C_1)(2\sigma_{xy} + C_2)}{(\mu_x^2 + \mu_y^2 + C_1)(\sigma_x^2 + \sigma_y^2 + C_2)},$$

where:  $\mu_x$  and  $\mu_y$  are the mean values of  $x$  and  $y$ , respectively.  $\sigma_x^2$  and  $\sigma_y^2$  are the variances of  $x$  and  $y$ , respectively.  $\sigma_{xy}$  is the covariance between  $x$  and  $y$ .  $C_1$  and  $C_2$  are small constants to stabilize the division, defined as:

$$C_1 = (K_1L)^2, \quad C_2 = (K_2L)^2,$$

where  $L$  is the dynamic range of the pixel values, and  $K_1, K_2 \ll 1$  are constants.

The SSIM value ranges from  $-1$  to  $1$ , where a value closer to  $1$  indicates higher similarity between the two signals.

These metrics provide a comprehensive evaluation for both the denoising and classification tasks, ensuring the reliability and quality of the results.

## D Model Analysis

### D.1 Q&A Analysis on Applying LLMs to Radio Signal Feature Extraction

The application of large language models (LLMs) to radio signal feature extraction is an emerging research direction that combines advancements in natural language processing (NLP) with signal processing techniques. Below is a detailed analysis of the challenges, advantages, and considerations involved in this novel approach.

#### 1. Why Use LLMs for Radio Signal Feature Extraction?

LLMs, such as GPT-2, BERT, and LLaMA, are designed to handle sequence data, making them versatile for tasks beyond textual data. Radio signals can also be represented as sequences (e.g., time-domain waveforms or frequency-domain representations). LLMs can be adapted to radio signal feature extraction due to their ability to capture long-range dependencies and complex patterns, which are crucial for analyzing radio signals.

Advantages:

1. Sequence Modeling: LLMs excel at processing sequential data, which aligns well with the inherent sequential nature of radio signals.

2. **Contextual Understanding:** LLMs can learn contextual relationships in signal features, such as frequency bands, modulation types, and time-domain patterns.
3. **Transfer Learning:** Pretrained LLMs on large datasets (e.g., self-supervised learning) can be fine-tuned for radio signal tasks with limited labeled data, reducing the need for large-scale datasets.
4. **Robustness to Noise:** LLMs can learn to generalize across noisy data, making them effective for real-world radio environments, where interference and noise are common.

#### Example Applications:

1. **Modulation Recognition:** Automatically identifying modulation schemes (e.g., AM, FM, QPSK) from signal data.
2. **Spectrum Analysis:** Extracting and classifying spectral features for interference detection or signal identification.
3. **Signal Detection:** Identifying weak signals buried in noise or interference using learned patterns.

### 2. Key Challenges in Applying LLMs to Radio Signals

Applying large language models (LLMs) to radio signal processing presents several unique challenges stemming from the fundamental differences between radio signals and text data. One of the primary difficulties lies in representing radio signals in a format compatible with LLMs. Common representations include raw IQ (In-phase and Quadrature) samples, which are complex-valued time-domain data; spectrograms, which transform signals into time-frequency representations; and feature vectors, which capture extracted characteristics like spectral peaks or bandwidth. Selecting the most suitable representation is critical, as it directly impacts how well the LLM can learn and process the signal's key features.

Another challenge is the high dimensionality of radio signals compared to text. High-bandwidth signals or long observation windows can result in sequences that are far longer than those typically encountered in NLP tasks. Feeding such long sequences into LLMs can significantly increase computational costs and memory requirements. Additionally, reducing the sequence length through downsampling or truncation risks the loss of essential information, which may degrade performance on tasks such as modulation recognition or spectrum analysis. This trade-off between computational efficiency and information retention is a key limitation when applying LLMs directly to raw signal data.

Finally, radio signals possess unique features that LLMs are not inherently designed to handle. For example, phase and amplitude relationships are critical for understanding modulation schemes but are not explicitly modeled in standard LLM architectures. Real-world radio environments also introduce noise and interference, which can act as adversarial inputs, further complicating the extraction of meaningful features. Moreover, the scarcity of large-scale, labeled radio signal datasets limits the ability to train or fine-tune LLMs effectively, unlike in NLP, where massive text corpora are readily available. These challenges highlight the need for specialized adaptations in data representation, model design, and training

strategies to fully leverage the potential of LLMs for radio signal feature extraction.

### LLM goes beyond dialogue: the potential of signal feature extraction

LLMs have traditionally been associated with natural language processing tasks, such as dialogue generation and text understanding. However, their versatility extends far beyond these applications. Recent advancements demonstrate that LLMs can be effectively applied to domains outside of text, including signal feature extraction, where they leverage their contextual understanding capabilities to identify patterns and relationships in complex datasets.

In the context of the RadioLLM framework, LLMs can process signal-related data by treating it as a sequence of features analogous to text tokens. This perspective enables models such as GPT-2, BERT, and LLaMA3 to extract meaningful features from signals, classify them, and even infer signal properties that are challenging to detect using traditional machine learning methods. For example, by training on domain-specific embeddings, LLMs can identify nuanced relationships between signal amplitude, frequency components, and modulation patterns, which are critical for tasks like signal classification or interference detection.

The potential of LLMs in signal processing is further enhanced by their scalability and ability to learn from large datasets. Unlike conventional methods, which often rely on handcrafted features, LLMs can automatically learn hierarchical representations, reducing the need for manual feature engineering. This makes them particularly well-suited for dynamic environments, where signals can vary significantly over time or across contexts. However, challenges such as high computational costs, long inference times, and the need for domain-specific fine-tuning remain barriers to widespread adoption.

Future research could explore how lightweight LLM architectures, such as distilled or quantized models, can be optimized for real-time signal processing tasks without sacrificing accuracy. Additionally, hybrid approaches that combine LLMs with traditional signal processing techniques could unlock new possibilities for efficient and robust feature extraction. This illustrates that the utility of LLMs extends far beyond dialogue systems, paving the way for innovative applications in signal analysis and beyond.

### Advancing CRT: How Radiollm Differs from Prior Work

RadioLLM represents a significant leap in cognitive radio technology (CRT), standing apart from prior approaches through its innovative design and comprehensive capabilities. Unlike traditional models that typically focus on a single task or rely on limited datasets, RadioLLM employs a hybrid and diverse dataset for pre-training, enabling it to capture a broader spectrum of signal features. This hybrid dataset incorporates a variety of signal types and conditions, allowing the model to generalize effectively across multiple scenarios.

Moreover, RadioLLM distinguishes itself by addressing multiple downstream tasks—classification, imputation, and denoising—within a unified framework. This all-in-one capability reduces the need for task-specific models, streamlining

the signal processing pipeline while maintaining high performance across tasks. By leveraging the powerful feature extraction capabilities of pre-trained large language models, RadioLLM bridges the gap between linguistic intelligence and radio signal processing, offering a versatile solution for complex signal environments.

Through this novel approach, RadioLLM not only advances CRT but also establishes a new benchmark for multi-task adaptability and efficiency in the field.